JOURNAL OF SPACECRAFT AND ROCKETS
Vol. 43, No. 1, January–February 2006

Fairing Noise Mitigation Using Passive Vibroacoustic Attenuation Devices

Steven A. Lane*
U.S. Air Force Research Laboratory, Kirtland Air Force Base, New Mexico 87117
and
Steven Griffin† and Robert E. Richard‡
Boeing-SVS, Albuquerque, New Mexico 87109

This work investigated the application of passive vibroacoustic attenuation devices (PVADs) for fairing noise mitigation. A PVAD is an integrated structural vibration mitigation device and acoustic damper. The PVAD was developed to provide low-frequency noise reduction and to be used as a supplement to acoustic blankets. This work presents modeling of the PVAD and composite cylinder test bed, simulations, optimization studies, experimental results using prototype devices, tests using two component devices, and tests using integrated PVADs on a 2.75-m composite cylinder. Two optimization schemes are presented: one based on radiation-mode analysis and the other using genetic algorithms. The measured experimental data supported conclusions from the model simulations and predictions. The performance of the integrated PVAD devices was better than that of individual components, and exceeded the performance of discrete masses and distributed mass loading. Narrowband reductions of 10 dB were demonstrated at low-frequency acoustic resonances. More than 6 dB of acoustic reduction was measured over the bandwidth of 50–125 Hz in the cylinder.

I. Introduction

VIBROACOUSTIC loads during launch pose a significant risk for payload launch survivability. Development of lighter weight, less damped composite fairings is expected to exacerbate the launch environment. The external acoustic levels during launch can exceed 160 dB, depending on the type of launcher and number of motors. There has been work to reduce the noise transmission into fairings, both passively and actively. Passive blankets provide acoustic damping in fairings. Blankets offer wide-band attenuation, although they are less effective at lower frequencies. Acoustic resonators have been successfully applied for narrowband attenuation in structural-acoustic systems such as cylinders and fairings.[1,2] Tuned mass dampers (TMDs) and tuned vibration absorbers (TVAs) have been used for vibration reduction in many applications.[3,4] These devices can also be used to reduce noise transmission through flexible systems.[5–10] Tuned vibration absorbers are typically single-degree-of-freedom devices that modify the mechanical input impedance of the vibrating structure. They are reactive devices with low damping that act over a narrow bandwidth to reduce the response of the structure at the design frequency. By inhibiting the noise transmission at the design frequency, structural-acoustic coupling and hence noise transmission can be reduced (at the design frequency). Tuned mass dampers are similar, but have more damping and can affect a wider bandwidth. They couple to the vibrating structure and change its behavior, particularly by adding damping to the structure, which reduces the amplitude of the vibration and noise transmission.

Work by Esteve and Johnson[11] and Osman et al.[12] investigated distributed vibration absorbers and Helmholtz resonators to provide noise reduction on the same sandwich composite cylinder test structure used in this work. Esteve et al. numerically and experimentally tested the effectiveness of lightweight distributed vibration absorbers and Helmholtz resonators that were tuned to the structural and acoustic resonances of the system. Their work showed that significant noise reduction could only be achieved by adding damping to both structural and acoustic modes that were resonant in the bandwidth of interest. Furthermore, they concluded that vibration absorbers and Helmholtz resonators were only effective if the structure and the acoustic cavity were lightly damped before adding the treatment.

Gardonio et al. provided an excellent theoretical development of fairing modeling and noise transmission and investigated the effects of "blocking masses" on noise transmission.[13] Their work provided a good discussion of prior work focusing on noise transmission through cylinders. Theoretical models of the in vacuo structural modes and the rigid wall acoustic modes were coupled using modal interaction analysis.[14] This analysis framework permitted the investigation of noise transmission sensitivity to various stiffness configurations, structural damping, acoustic damping, and disturbance loading conditions. A plane-wave disturbance model acting on the cylinder was used, and blocking masses of up to 8% of the cylinder's mass (i.e., 20 kg) were integrated into the model. The models were developed using parameters and data of the Ariane 5 payload fairing.

Gardonio investigated the noise reduction provided by adding blocking masses to the cylinder structure at discrete locations. The goal was to use the blocking masses to reconfigure the structural modes to reduce coupling between the incident acoustic waves, the cylinder, and the acoustic cavity. The performance achieved by incorporating 14 blocking masses (1.43 kg each) into the cylinder model was compared to the performance provided by increasing the structural mass by an equivalent amount (i.e., "smeared mass"). The results showed that significant performance was achieved using the discrete masses, while marginal performance was provided by the smeared-mass approach. The authors noted that, "... this study could be improved by developing an optimization approach which would indicate particular geometrical positions for the blocking masses that may give better results. ..."

Griffin et al. investigated active structural-acoustic control for fairing noise mitigation.[15] Those active control simulations implemented feedback controllers with proof-mass actuators, displacement sensors, and acoustic sensors, on a fully coupled state-space model of a small composite fairing. The simulated external

Received 12 October 2004; revision received 15 August 2005; accepted for publication 20 August 2005.

*Research Aerospace Engineer, Space Vehicles Directorate, 3550 Aberdeen Avenue SE. Senior Member AIAA.
†Enabling Technologies Lead, 4411 The 25 Way. Associate Fellow AIAA.
‡Vibrations and Control Analyst, 4411 The 25 Way. Senior Member AIAA.

disturbance was scaled to produce an approximate 140-dB open-loop exterior acoustic load. The mass of the controller was limited to 25% of the estimated fairing mass, which resulted in a limited number of proof-mass actuators available for control. Additionally, the closed-loop simulations imposed limits on the maximum voltage applied to the actuators. These restrictions were imposed so that the investigators could evaluate the feasibility of the control approach given realistic loads with reasonable controller constraints. It was found that the transmission through the bare fairing was reduced by 3.5 dB over 0–300 Hz by simply coupling 8 kg of proof-mass actuators with the fairing model. The closed-loop controllers (linear quadratic Gaussian) achieved, at best, approximately 4.2 dB of reduction of the noise transmission. Implementing multichannel feedback controllers on a real fairing was considered to be a difficult task and not worth the risk for only 4.2 dB of attenuation. Rather, it was theorized by the authors that optimally tuning the passive characteristics of structural vibration and acoustic response mitigating devices and using those with an acoustic blanket treatment would be more beneficial and introduce much less risk. It was from these observations that the passive vibroacoustic attenuation devices (PVAD) concept was originally developed.[16,17]

A PVAD is a combined structural vibration mitigation device and an acoustic damper. First, the PVAD modifies the modal response of the fairing through modal reconfiguration or simply by providing additional damping. This reduces the acoustic radiation of particular structural modes that are identified as efficient radiators.[18–20] Second, the PVAD simultaneously provides acoustic damping to specific acoustic resonances within the fairing using a passive diaphragm, membrane, or a damped acoustic resonator.

This paper will begin by reviewing some of the significant results from numerical studies, which included modeling, optimization, and performance predictions. This is followed by some of the early experimental work conducted on a composite cylinder to corroborate numerical simulations. Investigations of the behavior of separate structural and acoustic devices will be presented. Finally, integrated PVAD tests are presented with analysis of the results and some conclusions from the work.

II. Theory

A. PVAD Theory

The PVAD is composed of two parts, an acoustic damper component and a structural vibration attenuating component. Figure 1 gives a conceptual model of a PVAD device attached to a vibrating structure. The acoustic damper component uses a diaphragm, membrane, or simply a volume of moving air m_a to couple with the acoustic resonances of the fairing volume $\omega_{f,a}$. Diaphragms and membranes are often used for sound production, or reproduction, as in the case of a loudspeaker. Alternatively, Helmholtz resonators use a volume of air in the resonator neck as the moving mass. The stiffness k_a and damping d_a are provided by a flexure suspension (such as the "surround" or "spider" used in loudspeakers). If the diaphragm or membrane incorporates a sealed backing support structure, then the enclosed air volume in the support structure can contribute additional stiffness and damping. The resonance frequency and damping ratio for the acoustic damper part of the PVAD are then approximately given as

$$\omega_a = \sqrt{k_a/m_a}, \qquad \zeta_a = (d_a/2m_a)\sqrt{m_a/k_a} \tag{1}$$

The moving mass and the acoustic stiffness are tuned such that the device's resonance frequency is proximal to the desired fairing acoustic resonance frequency, that is, $\omega_a \approx \omega_{f,a}$. Damping is introduced to provide dissipation of acoustic energy in the coupled system. It will be demonstrated that damping is an important parameter for achieving good coupling and noise reduction.

The entire acoustic damper part of the device provides a moving mass m_s, which is attached to the vibrating structure via a flexible mounting. As in the case of a tuned-mass damper (TMD) or tuned vibration absorber (TVA), the moving mass m_s and flexible mounting are tuned to coincide with particular structural resonances $\omega_{f,s}$, which are to be attenuated. The flexible mounting provides stiffness k_s and can include springs, flexures, or even foam layers. The damping in the flexible mounting d_s determines whether the device behaves as a TMD, a TVA, or a combination of both. The resonance frequency and damping ratio of the "structural" part of the PVAD are approximately given by

$$\omega_s = \sqrt{k_s/m_s}, \qquad \zeta_s = (d_s/2m_s)\sqrt{m_s/k_s} \tag{2}$$

The suspension and moving mass are designed to couple with the target structural mode, that is, $\omega_s \approx \omega_{f,s}$. A reactive device ($\zeta_s < 1\%$) provides narrowband impedance loading, and a resistive device ($\zeta_s > 1\%$) provides a wider bandwidth of coupling and can add damping to the structural resonances if designed properly.

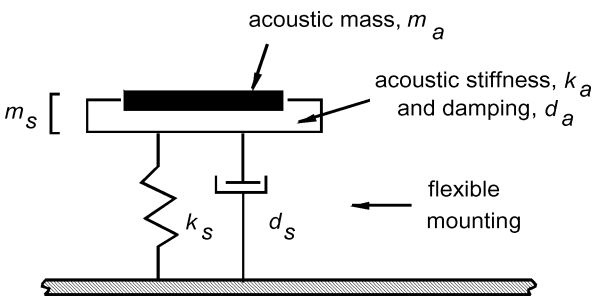

Fig. 1 Schematic of a PVAD consisting of an acoustic damper mounted via a flexible (tunable) base to a vibrating structure.

B. Air Force Research Laboratory PVAD Prototype Development and Testing

1. *Air Force Research Laboratory Prototype Development*

Several prototype devices were developed and tested during the course of this research program. The first prototype used an acoustic loudspeaker that was modified to have the desired resonance frequency and is shown in Fig. 2a. The loudspeaker had a 20.3-cm (8-in.)-diam diaphragm and was mounted in a small, sealed box that provided stiffness (air-spring effect) and some damping. The diaphragm and sealed box were mounted to the vibrating structure by three aluminum flexures that resembled leaf springs. The loudspeaker was used as a passive device, that is, no voltage was applied. The electrical leads of the loudspeaker were connected to a resistor, or in some cases, shorted. Using a resistor or shorting the leads adjusts the electromechanical damping of the device and was used to tune the mechanical impedance and coupling of the device to the acoustic volume.

A later PVAD prototype, shown in Fig. 2b, used a Helmholtz resonator approach, having a moving air mass as opposed to a diaphragm or membrane. Damping of the resonator was achieved by placing flow-resistant material in the neck of the resonator. The acoustic damper was constructed of acrylic and PVC materials. The acoustic damper was attached to the vibrating structure by a foam layer. The foam layer (Melamine foam) provided both stiffness and damping, which offered a tunable flexible mounting and introduced very little mass. The overall mass of the device in Fig. 2b was much less than that of the diaphragm device of Fig. 2a.

2. *Air Force Research Laboratory PVAD Prototype Testing*

A light-weighted version of a PVAD using a diaphragm (as shown in Fig. 2a) was tested in a one-dimensional acoustic cylinder. The cylinder had a rigid, plywood cap on one end and a flexible panel on the other. A schematic of the test bed is shown in Fig. 3. The first three acoustic resonances of the cylinder were 79, 161, and 241 Hz. The first three resonance frequencies of the panel were determined using impact hammer tests to be approximately 112, 130, and 200 Hz. The flexible panel provided a dynamic transmission path for the external disturbance, which was generated by a subwoofer approximately 1 m from the cylinder. The effect of the PVAD was measured by comparing the transfer function measured between a microphone inside of the cylinder and a microphone outside of the cylinder.

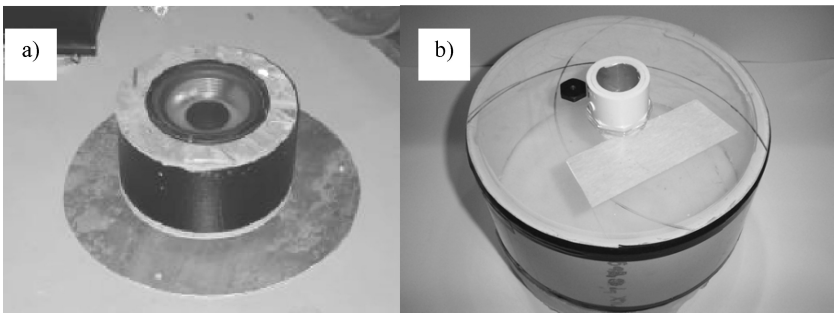

Fig. 2 Prototype PVAD devices: a) the passive diaphragm device and b) the Helmholtz resonator device.

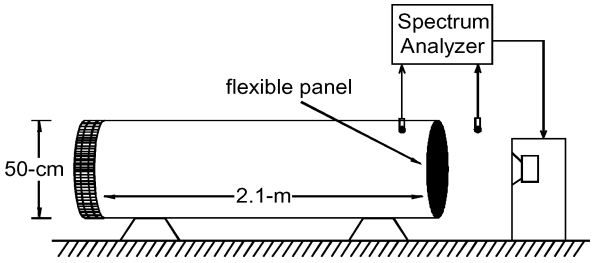

Fig. 3 Cylinder test bed used for prototype PVAD testing.

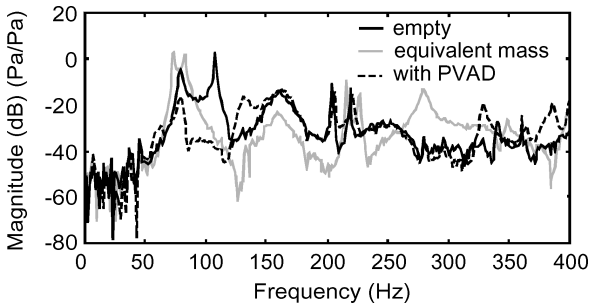

Fig. 4 Noise transmission results from a PVAD prototype in a one-dimensional acoustic cylinder.

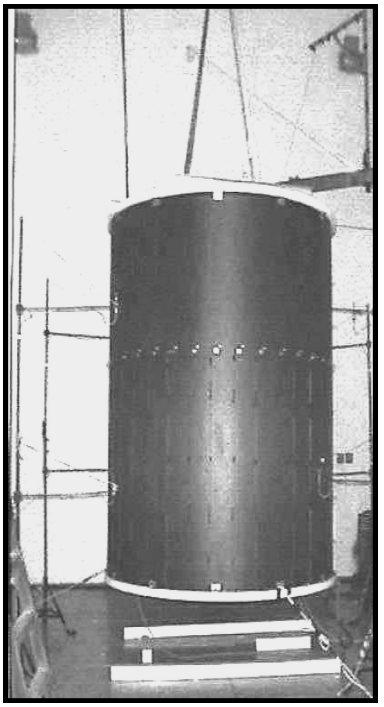

Fig. 5 Composite cylinder used for development, testing, and evaluation.

The PVAD was designed to have an acoustic resonance at 80 Hz and a (damped) structural resonance near 110 Hz. The acoustic and structural damping were between 3 and 5% of critical. The total mass of the PVAD was approximately 0.6 kg (1.5 lb). The measured results are given in Fig. 4. The first measurement was of the cylinder transmission with no PVAD device and clearly shows the first acoustic and panel resonance. The PVAD reduced the first acoustic resonance by over 15 dB and first panel resonance by about 40 dB. The rms reduction over the 400-Hz bandwidth was computed to be 8.1 dB. Also shown in Fig. 4 is the effect of attaching an aluminum block (with mass equivalent to the mass of the PVAD) to the panel with no flexures. The additional mass significantly reduced the response at the panel resonance, but worsened the response at the acoustic resonance. The computed reduction over the 400-Hz bandwidth with the equivalent mass was only 1.1 dB.

Further experimental testing using the aluminum cylinder indicated that damping values between 5 and 7% provided optimal coupling (and attenuation) between the PVAD and the low-frequency acoustic resonances. The optimal damping for the structural suspension was found to be around 5% but varied with respect to the panel dynamics (mass, stiffness, and damping). Testing showed that the total volume of the acoustic resonator needed to be at least 1% of the total acoustic volume to provide significant performance.

C. Numerical Studies and Optimization on a Composite Cylinder

The successful demonstration in the lab using the aluminum cylinder led to expanded modeling and optimization efforts. The test structure considered in the following numerical and optimization studies was a composite cylinder fabricated by the Boeing Company and made available to the Air Force Research Laboratory and Virginia Polytechnic Institute and State University (Virginia Tech) for conducting fairing noise control research. In the following, the cylinder description will be given, and then the optimization studies will be presented. The first set of studies used a radiation-mode approach for placing the PVADs, wherein control effort is focused on those structural modes that efficiently couple with acoustic modes. In the second study, a genetic-algorithm approach was used to optimize PVAD locations and design parameters. In both studies, fully coupled structural-acoustic models of the composite cylinder and PVADs were used. Disturbance loads used for simulations were scaled to realistic launch loads (130–140 dB).

The composite cylinder provided by the Boeing Company for this research is shown in Fig. 5. The cylinder was a sandwich composite, weighing 80 kg, with height of 2.75 m, and inner radius of 1.2 m. End caps were fabricated for the cylinder from plywood (about 10 cm thick) and reinforced with aluminum I beams. The thickness of the face sheet/honeycomb shell was approximately 6 mm. Several design iterations were performed to reduce noise transmission through the end caps. Threaded rods on the outside of the cylinder connected the two end caps and kept the end caps firmly attached to the cylinder. A hatch on the top end cap was used for entering into the cylinder to instrument the interior.

D. Preliminary Numerical and Optimization Studies

In the first numerical study, the effects of the structural damper part of the PVAD were investigated as a function of mass, location, damping ratio, and number of devices. This was followed by studies using both a structural damper and a diaphragm-type acoustic damper. Two diaphragm diameters were modeled, 15.25 cm (6 in.) and 30.5 cm (12 in.).

1. Model Development

A fully coupled finite element model of the composite cylinder was developed, and the resulting eigenvectors and eigenvalues were imported into Matlab®,[21] where state-space models were developed for simulations. The in vacuo structural model and the rigid-wall acoustic model were coupled using modal interaction analysis.[22] The mesh spacing was defined to allow computation of the interior acoustic response to approximately 250 Hz (more than five nodes per acoustic wavelength). The PVADs were coupled with the structural and acoustic models of the cylinder. This was accomplished using feedback between the PVADs and both the structural nodal coordinates and the acoustic nodal coordinates. The model was developed using the geometry of the cylinder and the expected structural material parameters, as no data were available. Damping ratios for the acoustic and structural subsystems were 1.5 and 1%, respectively.

2. Disturbance Model

Nodal point force inputs were used as the disturbance loads in these simulations and applied to the structural nodal points. The disturbance inputs were only applied to a subset (30%) of the cylinder nodes (chosen arbitrarily) on the cylinder to reduce computational time and to create asymmetric loading. Loading at each node was uncorrelated random noise.

3. Performance Metric

The internal acoustic response was computed at every interior node, root sum squared over frequency, and spatially averaged over all nodes. The noise reduction was computed as the ratio of the averaged interior acoustic response without devices to the response with devices:

$$\text{Noise Reduction (dB)} = 20\log_{10}(P_{\text{no devices}}/P_{\text{with devices}}) \qquad (3)$$

4. Optimal Positioning

A method to select "optimal" locations for PVADs was developed by the authors with a direct experimental implementation. This approach was based on an observation from radiation-mode analysis that structural-acoustic nodes with both high-pressure and high-out-of-plane displacement are good locations for structural-acoustic actuators or PVADs. To find the optimal locations, the "bode" command in MATLAB was used over the frequency range of interest (0–250 Hz) to get the frequency response functions with the disturbance as an input and the pressures and out-of-plane displacements as outputs at all of the structural and acoustic nodes. The real parts of the structural frequency response functions were maximum at structural modes, while the imaginary parts of the acoustic frequency response functions were maximum at these locations. To find the maximums of both and to maintain the phase information, the product of the real structural frequency response functions and the imaginary acoustic frequency response functions were calculated. At each node, the maximum of the computed product was calculated along with the frequency where the maximum occurred. These maxima were rank ordered, and the top locations were selected as locations for PVADs. The end caps were modeled as rigid and excluded from the set of possible PVAD attachment points.

5. TMD Effect and Mass Loading Effect

The first part of this study considered the tuned mass damper effect alone, which is equivalent to shunting the acoustic damper part of the PVAD. A total of 100 optimal locations were selected, and performance was computed for the addition of the devices, each having mass of 175 g (0.386 lb) and structural damping of 10% of critical. (These values were representative of what would be fabricated later for laboratory experiments.) The stiffness of each PVAD was defined so that the frequency of each device corresponded to the structural-radiation mode for which it was assigned by the rank-ordering process. Figure 6 shows the power-spectral-density plots of the spatially averaged interior acoustic responses with and without the devices attached to the cylinder wall. The reduction over the bandwidth (0–250 Hz) between the "with PVAD" and the "without PVAD" cases was computed to be approximately 6.7 dB. The first mode, where significant increase (spillover) occurred, corresponded to the fundamental acoustic mode of the coupled model.

Table 1 Summary of numerical results for various TMD cases

Case	Number of devices	Mass, g	Damping, %	Reduction, dB	Mounting
1	100	175	10	6.7	Flexible
2	100	175	10	2.8	Rigid
3	100	87.5	10	5.9	Flexible
4	100	87.5	10	2.1	Rigid

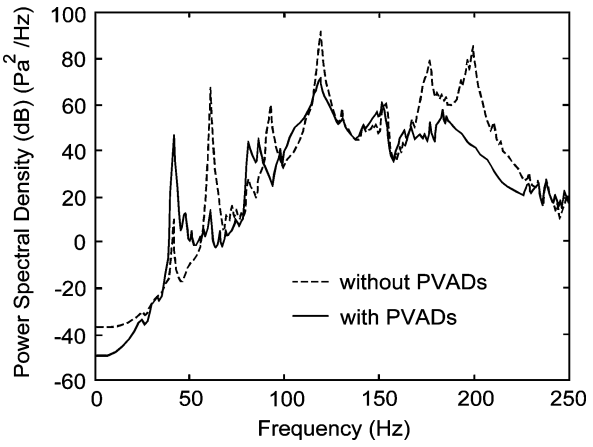

Fig. 6 Spatially averaged interior pressure spectra of cylinder simulations using 100 PVADs.

Other simulations were computed using a lighter device of 87.5 g (0.193 lb) and using the equivalent mass with no flexible suspension (rigid attachment), equivalent to the blocking masses investigated by Gardonio. The results are summarized in Table 1. The reduction computed using the lighter devices (case 3) was 5.9 dB. For the cases of the rigidly attached masses, 2.8 dB of reduction was computed for 175-g masses and 2.1 dB for 87.5-g masses.

The positions of the devices were varied to determine the sensitivity of performance with respect to location; however, little effect was measured ($\sim$1 dB). This indicated that the performance of the structural part of the PVAD was not very sensitive to placement when such a large number of devices were used.

6. Investigating Damping Ratio

Using case 1 in Table 1, the variation of performance as a function of the suspension's damping ratio was investigated. The damping ratios of all PVADs were varied uniformly from 0.1 to 25%. Figure 7 presents a plot of the noise reduction (with PVADs to without PVADs). The results indicate a maximum reduction at between 5 and 10% damping. At very low damping ratios, the noise reduction decreased at a sharp rate as the ability of the device to dissipate energy was diminished. Above 6% damping, the computed noise reduction decreased, but at a slower rate.

7. Investigating the Number of Devices

In the next simulations, the number of devices was varied (using 175-g devices with 10% damping). The computed noise reduction is given in Fig. 8. There is no obvious optimum; in fact, performance

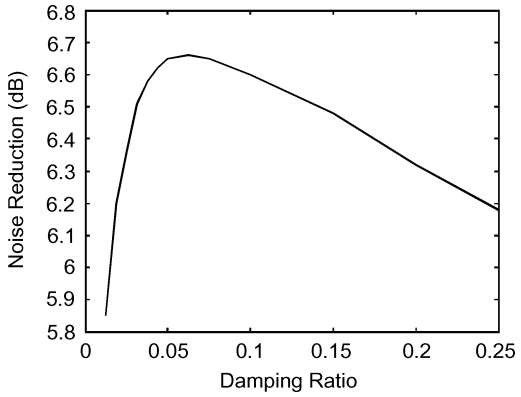

Fig. 7 Computed noise reduction as a function of the suspension damping.

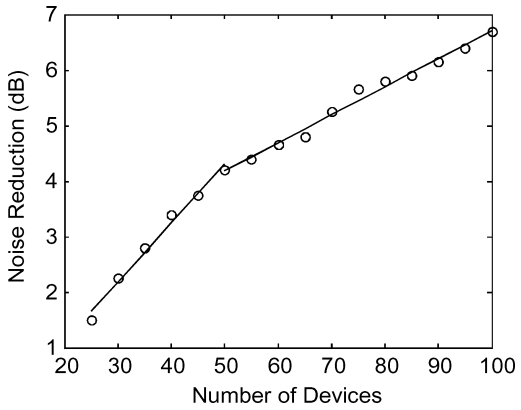

Fig. 8 Computed noise reduction as a function of the number of devices.

was nearly linear with the number of devices used. However, it appears as though the slope of the curve begins to gradually decrease, indicating that the rate of performance increase can diminish with increasing number of devices.

8. Adding the Acoustic Damper

Next, simulations were conducted with diaphragm-type acoustic absorbers added to the devices used in case 1 of Table 1. Diaphragms with diameters of 30.5 cm (12 in.) and 15.25 cm (6 in.) were investigated for all 100 devices. This represented 7.3 and 1.82 m^2 total surface area, respectively, which was approximately 34 and 8.5% of the total cylinder wall surface area, respectively. (The 30.5-cm-diam case was unrealistic because neighboring node locations for the PVADs created overlapping of the diaphragms.) The diaphragm mass was selected to be 45 g (for both cases), which was consistent with a typical loudspeaker. Damping of the diaphragm suspension was defined to be 5%. The stiffness of the diaphragm suspension was defined such that the resonance frequency of the acoustic damper corresponded to the acoustic mode proximal to the structural-acoustic resonance assigned by the rank-ordering process. The diaphragm absorbers were coupled into the model as spring-mass dampers in the finite element model. Figure 9 presents the power spectral density plots of the spatially averaged interior responses. The devices provided significant attenuation across the bandwidth above 60 Hz. The addition of the 30.5- and 15.25-cm absorbers yielded a total noise reduction of approximately 11.3 and 10.1 dB, respectively. At low frequency, the addition of acoustic absorbers increased transmission. It is believed that this was caused by the addition of radiating surfaces with significant motion at low frequency. Note that the response of the fundamental acoustic mode (at about 45 Hz) was very low without any devices. Hence, it was not targeted by the rank-ordering optimization process.

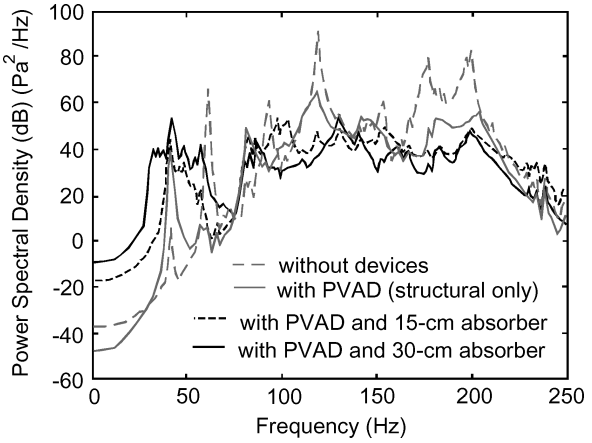

Fig. 9 Spatially averaged interior pressure spectra of cylinder simulations using 100 PVADs with diaphragm-type acoustic absorbers.

E. Genetic-Algorithm Optimization Studies

Optimization studies were performed using genetic algorithms[23–28] to compute optimal mass, stiffness, and damping parameters of PVADs attached to a fully coupled structural-acoustic cylinder model. Genetic algorithms were also used to search for optimal PVAD mounting locations. Simulations were conducted using various numbers of PVADs. Genetic algorithms offer a powerful optimization tool when the parameter search space is large. Genetic algorithms require many cost function evaluations in order to converge to a solution, which proved to be very time consuming for large parametric studies. Thus, innovative approaches were developed to make the problem manageable. A technique called modal threshholding was used to eliminate structural modes that did not couple well with the acoustic cavity. By removing these ineffective radiation modes, the sizes of the matrices were reduced, and cost functions were calculated faster. Parallel processing methods were also developed to improve computation speed. Both binary and integer representations of the chromosomes were implemented. It was found that convergence was twice as fast with the integer string representations.

The cost function used by the genetic algorithm was the acoustic potential energy, which is a function of frequency and is given by

$$E(\omega) = \sum_{i=1}^{N} \Lambda_i |p_i(\omega)|^2 \tag{4}$$

where Λ_i is the modal volume for mode i, N is the number of modes in the coupled model, and $p_i(\omega)$ is the modal participation factor for acoustic mode i at frequency ω. The performance index J was defined as the sum of potential energies across the frequency range of interest:

$$J = \sum_{\omega=\omega_1}^{\omega_2} E(\omega) \tag{5}$$

For these simulations, the cost function was computed over 50–300 Hz, although the models extended beyond 300 Hz. The performance was computed only over this range because it was desired to optimize the PVADs for low-frequency noise mitigation.

1. Modeling Effort

Finite element models of the in vacuo cylinder and rigid-wall acoustic volume were developed using ANSYS.[29] The models were tuned to match resonance frequency values measured from the composite cylinder. The eigenvalues and eigenvectors were loaded into MATLAB, and the in vacuo structural and rigid-wall acoustic models were coupled using a modal interaction approach. The coupled model extended to approximately 600 Hz and included 360 structural modes and 327 cavity modes. The first five acoustic modes occurred at approximately 63, 83, 104, 125, and 131 Hz. Proportional damping was included in the structural modes (0.5%) and

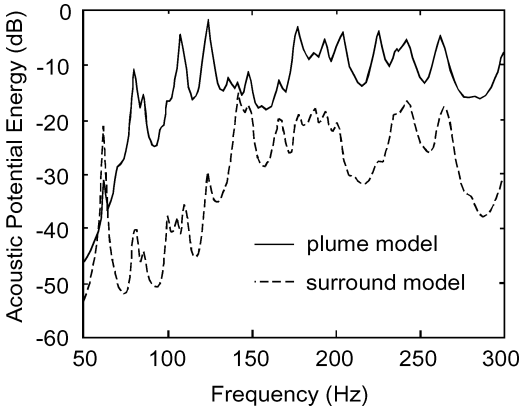

Fig. 10 Comparison of computed acoustic potential energy for simulated directional (plume) loading and for uniform nodal point force loading (no PVADs).

acoustic modes (1%). The TMD part of the PVAD and the acoustic damper (AD) part of the PVAD were coupled into the model using a mathematical framework that permitted multiple-degree-of-freedom devices, which captured torsional vibration of the TMD part, and multiresonance behavior of the acoustic damper part.

2. Disturbance Modeling

Two types of external disturbance loads were modeled and used in these simulations. The first was a distributed nodal loading of bandlimited random noise, which was scaled to an equivalent exterior load of about 130 dB. The other loading condition was a line source at one side of the cylinder, similar to what a thrust-plume might produce. This provided an asymmetric load condition. Figure 10 compares the internal acoustic response for the nodal point force inputs (denoted as "surround" in Fig. 10) and the response from the line source disturbance (indicated as "plume"). Note that the response from the line source was much greater, likely because the load was asymmetric and the disturbance coupled with the cylinder more effectively. Both disturbance models were used in simulations, and each led to similar results and conclusions (because noise reduction is a relative measurement).

3. Results: Position and Parameters for the 5 PVAD Case

The first set of simulations used the nodal force disturbance model (surround) and diaphragm-type PVADs. The parameter space included the mass, stiffness, damping, and nodal positions for five PVADs. The parameter space for the TMD moving mass (i.e., mass of the acoustic damper) was limited to 5–500 g. The mass of the acoustic diaphragm was also limited to 5–500 g. Damping ratios for each part were limited to 1 to 25%. The natural frequency of each part (thus defining the stiffness) was allowed to vary from 10 to 500 Hz. All structural nodes of the cylinder were included in the parameter space as potential device locations. Multiple optimizations were conducted using this parameter set. Convergence was achieved after 600–700 generations. The solutions were reasonably intuitive. The mass of the TMD parts tended towards the upper limit of about 500 g per device. The acoustic mass (diaphragm) tended towards the minimum of 5 g per device. The frequencies of the TMD suspensions tended toward the 200–300-Hz frequency range, where the internal response was the greatest. The frequencies of the acoustic dampers tended to this same frequency range and to low-frequency acoustic resonances that exhibited large response (i.e., the first longitudinal acoustic mode). The damping of the TMD suspensions tended to the maximum value of 25% (of critical), whereas the damping of the acoustic dampers tended to 3–6%. The locations of the PVADs in the converged solutions typically were closely distributed about the middle of the cylinder. However, it was noticed that PVADs targeting the longitudinal acoustic mode (acoustic resonance of 63 Hz) were positioned near the bottom or top of the cylinder. This was reasonable because this was where the pressure antinodes occurred for the fundamental acoustic mode. The average reduction of the acoustic potential energy for the converged solutions was 3.2 dB. The variation from the mean was typically less than 0.5 dB. Figure 11 presents the acoustic potential energy function for the cylinder with and without the devices for a representative simulation run.

Table 2 PVAD parameters of the converged solutions (18,000 generations)

Number of PVADs	Component	f_{min}, Hz	f_{max}, Hz	f_{mean}, Hz	ζ_{min}	ζ_{max}	ζ_{mean}
10	TMD	87	341	232.8	13	25	20.5
	AD	83	296	249.7	3	20	6.9
20	TMD	125	331	230.3	11	25	18.4
	AD	40	161	94.6	3	25	14.1
30	TMD	88	335	237.5	6	25	19.4
	AD	25	502	305	3	25	12.2

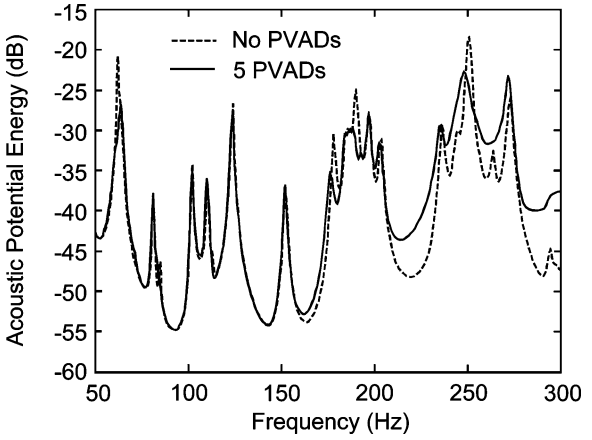

Fig. 11 Acoustic potential energy reduction using five optimized PVADs.

4. Results: Varying Number of Devices

Additional simulations were conducted using 10, 20, and 30 PVADs. These simulations implemented models of Helmholtz-resonator-type acoustic dampers, that is, a volume of air constituted the moving mass as opposed to a diaphragm. This was done because the previous optimizations tended towards a very low value for the moving mass. The moving mass of the TMD part was fixed at 450 g, and the moving mass of the air was defined as 10 g. (The value of 10 g was assumed a reasonable estimation of the moving mass for prototype devices being studied.) The genetic algorithm was used to determine optimal values for the resonance frequencies, damping ratios, and device positions. The optimization parameter space for the resonance frequencies of the structural and acoustic parts of the PVAD was limited to 11–510 Hz. The parameter space for the damping ratios for each part was limited to 1–25%. For these simulations, the plume disturbance model was used. Convergence was achieved for each case after about 18,000 generations. The cost function was computed over the bandwidth of 50–300 Hz.

The results are summarized in Table 2, where TMD indicates the values of the structural parts of the PVADs, and AD indicates the acoustic damper parts of the PVADs. Table 2 gives the minimum, maximum, and mean resonance frequencies and damping ratios for PVADs in a given test case. The converged solutions exhibited a wide range of device frequencies and damping ratios. The results did not exhibit general trends, except that the average acoustic resonator damping was consistently less than the average TMD damping. Such was the case for PVAD locations. It appears that for a small number of PVADs (five) the optimal positions for those PVADs tended to consistent locations, that is, the ends and the middle. However, as the number of PVADs increased, the locations of the devices did not seem as exclusive, and the converged locations were scattered all over the structure.

The computed cost function reductions were 2.9 dB (10 PVADs), 3.2 dB (20 PVADs), and 4.4 dB (30 PVADs). Figure 12 presents the

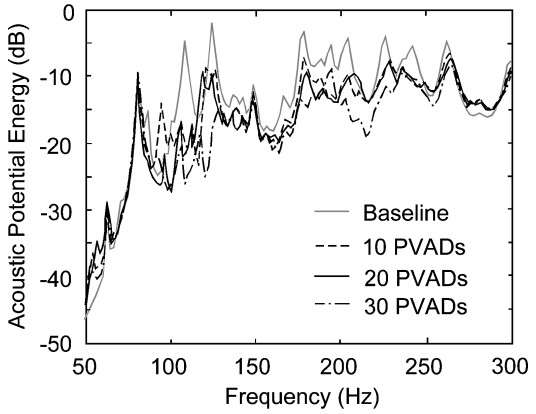

Fig. 12 Acoustic potential energy for the converged optimizations using 10, 20, and 30 PVADs.

acoustic potential energy as a function of frequency for the three test cases and the baseline (no PVADs). Most of the dominant resonances were reduced, except for the fundamental acoustic mode, which was not as dominant as in the previous simulations (Fig. 11). The reduction of noise transmission from an equivalent smeared-mass model was not computed for each case.

III. Model Validation and Characterization Measurements

A. Introduction

Experimental tests were conducted on the composite cylinder to validate models and to better understand the dynamics in the structural-acoustic transmission path. These tests identified potential "target" structural-acoustic modes for the PVADs. Testing was conducted in a semireverberant acoustics laboratory at Virginia Tech to measure the acoustic frequency response functions from a single subwoofer to several microphones mounted within the cylinder and accelerometers attached to the cylinder. Measured resonance frequencies, damping ratios, and coupling were compared to finite element model predictions from the model developed and discussed in the first study of the preceding section. The finite element model employed a distributed loading (random noise inputs) at many arbitrary nodes of the structural, whereas our test system used a single volume-velocity source in a semireverberant laboratory. (It was of practical importance to use a single disturbance source, as this permitted the direct measurements of frequency response functions from the single driver to the internal microphones). Remarkably, there was significant similarity between the measured and predicted responses, which indicates that the distributed loading generated in the laboratory was well approximated by the distributed loading that was modeled.

B. Experimental Setup

The cylinder was mounted on a framed platform about 0.4 m off of the floor. Access to the cylinder interior was achieved through a removable port on the top end cap. The disturbance subwoofer was manufactured by Radian Audio, had a 30.5-cm (12-in.)-diam diaphragm, and was mounted in a sealed cabinet (0.11 m^3). The disturbance source was placed approximately 3 m from the cylinder and 0.5 m off of the floor. The disturbance was measured to be approximately 109 dB (relative to 20 μPa) at 20 cm from the cylinder exterior. A small accelerometer was attached to the subwoofer diaphragm and used as a reference for the transfer function measurements [PCB Piezotronics accelerometer model 352B10; sensitivity = 10 mV/g; frequency range = 2–10,000 Hz (±5%); mass = 0.5 g].

Collocated accelerometers [PCB Piezotronics accelerometer model 320C03; sensitivity = 10 mV/g; frequency range = 1 Hz–6 kHz (±5%)] and microphones [Radio Shack electret microphone model KUC1723-6730; sensitivity = 80 mV/Pa; frequency range = 20 Hz–15 kHz (±5%)] were placed on the cylinder wall to measure the responses at the cylinder's interior boundary surface. The collocated pressure and acceleration was measured on the cylinder wall over an equally spaced grid of 256 points (32 circumferential positions by eight axial positions). It was desired to narrow our focus to structural modes that showed up in these transmission measurements; thus, a more thorough modal analysis was not attempted. Five other microphones [PCB Piezotronics ICP microphone model 130C10; sensitivity = 25 mV/Pa; frequency range = 20 Hz–7 kHz (±1 dB)] were placed throughout the interior of the cylinder on a microphone "tree."

These tests used a 1-s duration burst chirp (40–200 Hz) with a 1-s delay between chirps and a 1.5-s acquisition widow (to capture the full response). For each measurement, the coherence was checked to ensure data quality. The sensor cables were pulled through a small port through the top end cap, which was otherwise plugged as much as possible to prevent flanking. The temperature inside the cylinder was regulated to remain $24 \pm 1.6^{\circ}$C during testing.

C. Experimental Results

The measured resonance frequencies matched the finite element model predictions reasonably well. It was possible to tune the model to achieve better correlation over the 200-Hz bandwidth. Figure 13 presents the spatially averaged response at the wall microphones, and Fig. 14 presents the averaged response at the interior tree microphones. The wall microphones indicated dominant resonances at 63, 84, 103, 110, 120, 155, 183, and 196 Hz. The interior microphones showed additional significant modes at 125 and 148 Hz. The damping of the modes appeared to vary. A significant structural resonance occurred below the fundamental acoustic mode at 45 Hz. The response at this frequency seemed strongly dependent upon the orientation of the cylinder with respect to the disturbance source. The models did not predict the 45-Hz structural mode or the relatively large contribution at 196 Hz. (The cylinder properties were anisotropic, and the tie-rods used to secure the cylinder to the test frame did not create a consistent compression load around the

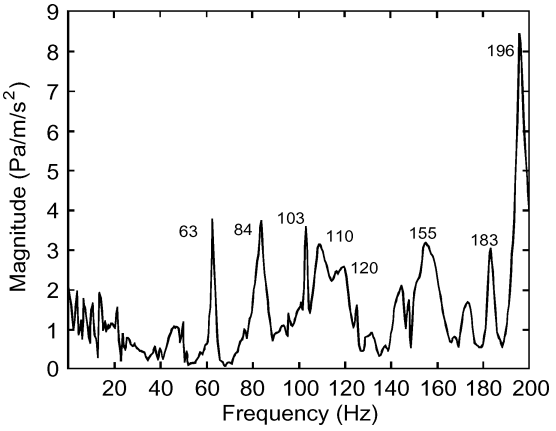

Fig. 13 Spatially averaged wall microphone pressure amplitude.

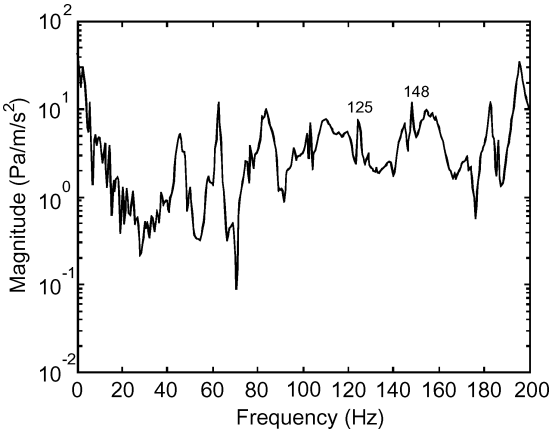

Fig. 14 Spatially averaged tree microphone pressure amplitude.

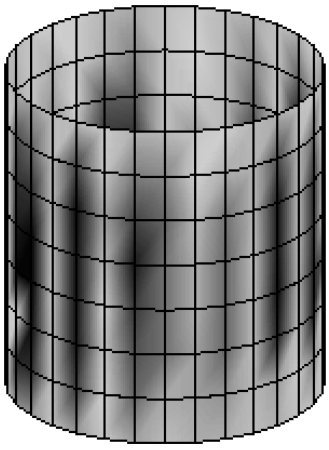

Fig. 15 Measured cylinder vibration at 63 Hz.

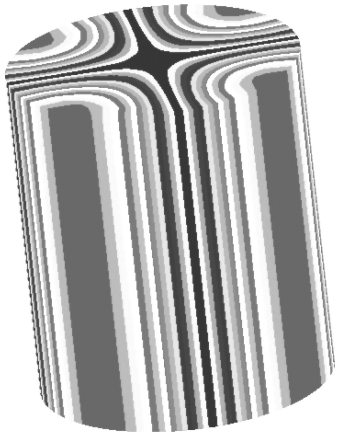

Fig. 16 Finite element model prediction of the acoustic mode at 103 Hz.

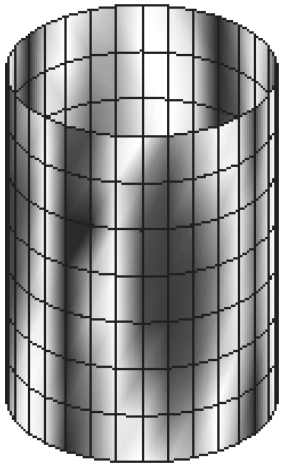

Fig. 17 Measured wall microphone data at 103 Hz.

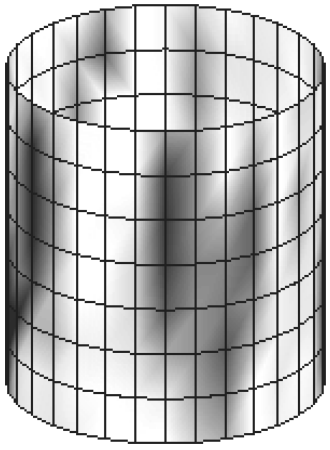

Fig. 18 Measured accelerometer data at 103 Hz.

cylinder, which resulted in varying boundary conditions around the cylinder. As a result, the orientation of the cylinder with respect to the direct field of the driver did indeed effect the structural-acoustic transmission.)

The measured data indicated that the fundamental acoustic resonance frequency at 63 Hz appeared to line up fairly closely with a structural mode. The measured acceleration data are plotted in Fig. 15 for 63 Hz, and they appear to indicate a circumferential mode shape. This would seem to be a good frequency to target with both acoustic dampers and structural attenuation devices.

Another example of an acoustic mode that correlated well with model predictions was at 103 Hz. The sensor data indicate modal patterns for both the structure and the acoustic volume at this frequency. Figure 16 shows the predicted acoustic mode shape at this frequency, Fig. 17 shows the measured microphone data, and Fig. 18 shows the measured accelerometer data. Clearly, this frequency would be a good design frequency for a structural-acoustic device.

Although resonance frequencies were closely predicted by the finite element model, prediction of transmission (i.e., coupling with an external disturbance) was less accurate. The orientation (rotation) of the mode shapes was dependent on disturbance source location. Several lightly damped structural-acoustic frequencies were identified as potential design points for PVADs. It was observed that in many instances positions of high out-of-plane motion did correspond to large acoustic pressure responses. Variations of the resonance frequencies and apparent damping ratios were observed between the many measured transfer functions. Although large ensembles of data were analyzed for the results given in Figs. 13 and 14, the variation about the mean resonance frequencies was generally 2–3 Hz.

IV. PVAD Component Testing

A. Introduction

It was decided that the first noise reduction tests on the composite cylinder would use separate damped Helmholtz resonators, TVAs, and TMDs. Testing of separate devices before development of an integrated device was viewed as a necessary risk-reduction step. It was estimated that testing could be done using separate devices at a fraction of the cost of developing integrated PVADs. Also, using separate devices allowed assessment of the individual devices on noise transmission reduction.

Damped Helmholtz resonators were designed to target four dominant acoustic modes at 63, 84, 183, and 196 Hz. Damped Helmholtz resonators were used instead of diaphragm absorbers as a result of the genetic-algorithm simulations, which repeatedly tended to minimize the "acoustic" moving mass. They were constructed from PVC materials and damped ($\zeta \sim 5\%$) by putting wire mesh in the resonator neck. Ten acoustic dampers were designed for each frequency.

Tuned vibration absorbers and tuned mass dampers were designed and fabricated by CSA Engineering.[§] TVAs were designed for 63 and 84 Hz, and TMDs were designed for 196 Hz. Six devices were designed for each frequency. The mass of each device was approximately 260 g. The damping ratios of the TVAs were $\zeta = 0.005$ and for the TMDs were $\zeta = 0.062$.

B. Experimental Setup

These tests were performed in the same acoustics lab at Virginia Tech using the same setup, disturbance source, and reference signal as were used for characterization tests. Five accelerometers [PCB Piezotronics accelerometer model 320C03; sensitivity = 10 mV/g; frequency range = 1 Hz–6 kHz (±5%)] and five microphones [Radio Shack electret microphone model KUC 1723-01-6730; sensitivity = 80 mV/Pa; frequency range = 20 Hz–15 kHz (±5%)] were placed arbitrarily on the cylinder (interior) wall, and six [PCB Piezotronics ICP microphone model 130C10; sensitivity = 25 mV/Pa; frequency range = 20 Hz–7 kHz (±1 dB)] were mounted to the microphone tree. The disturbance load was approximately

[§]Data available online at www.csaengineering.com [cited 30 December 2005].

110 dB. Burst chirps (40–200 Hz) were used as the disturbance signal as in the previous tests. Performance of the various devices was measured as the ratio of the spatially averaged and frequency averaged signals as given in Eq. (3). The acoustic dampers were placed on the floor of the cylinder, which allowed good coupling with the acoustic volume without mass-loading the cylinder wall. The TVA and TMD devices were attached to the cylinder by affixing a mounting base to the cylinder wall with epoxy and then attaching the devices to the base via a threaded screw. The devices were placed on the cylinder at locations distributed around the circumference and at various heights, locations that corresponded to relatively high out-of-plane motion for the particular design frequency. Because nearly six months had passed since the previous characterization measurements, transfer functions were remeasured to identify any changes in the modal behavior: there were no significant changes. The devices were positioned so that the mode shape could not simply rotate to avoid coupling with the devices. Each test included 30 averages, and only data with coherence greater than 90% were retained. Because the disturbance source rolled off below 40 Hz (subwoofer limitation), the performance was computed only over 50–200 Hz. The uncertainty in the following noise reduction data was estimated to be less than ± 0.01 dB based on test-to-test repeatability (experimental uncertainty) and equipment specifications (measurement uncertainty). Many data sets were averaged, and good data quality was obtained using the burst chirps, both factors that contributed to the low experimental uncertainty. The tests were conducted over a two-day period, and the setup and test environment were held consistent as possible.

C. Experimental Results

Many different combinations of devices were tested: several will be discussed here, and the results are summarized in Table 3. The 63-Hz acoustic dampers attenuated the target mode by nearly 15 dB. Over the 50–200-Hz bandwidth, reduction was computed to be 0.49 dB at the wall microphones and 0.07 dB at the tree microphones. There was no measured reduction at the accelerometers. Using all 40 dampers provided 1.11-dB of attenuation at the wall microphones and 0.38 dB at the tree microphones. The averaged accelerometer response increased by −0.03 dB. The spatially averaged transfer function for this test case (using wall microphones) is given in Fig. 19. Approximately 15.5 dB of reduction was measured at 63 Hz, 1 dB at 84 Hz, 6 dB at 183 Hz, and 8 dB at 196 Hz. Reductions were also measured at 125 and 148 Hz, with only slight spillover at a few frequencies.

Using the TVAs tuned for 84 Hz with no resonators produced 0.92 dB of reduction at the wall microphones and 0.52 dB at the accelerometers, but increased the response at the tree microphones by 0.31 dB. Combining all acoustic resonators with the 84 Hz TVAs provided 1.63 dB of reduction at the wall microphones, 0.72 dB at the tree microphones, and 0.85 dB at the wall accelerometers. Similar results were measured using all acoustic dampers with the 63-Hz

Table 3 Measured reduction from cylinder tests using acoustic dampers, TVAs, TMDs, and blocking masses

	Reduction, dB		
Test case	Wall microphones	Wall accelerometers	Tree microphones
63-Hz acoustic dampers	0.49	0.00	0.07
All acoustic dampers	1.11	−0.03	0.38
84-Hz TVAs only	0.92	0.52	−0.31
All acoustic dampers and 84-Hz TVAs	1.63	0.85	0.72
All acoustic dampers and 63-Hz TVAs	1.75	0.63	0.72
All acoustic dampers and 196-Hz TMDs	1.56	0.87	0.97
All acoustic dampers and 6 blocking masses	1.49	−0.63	0.72

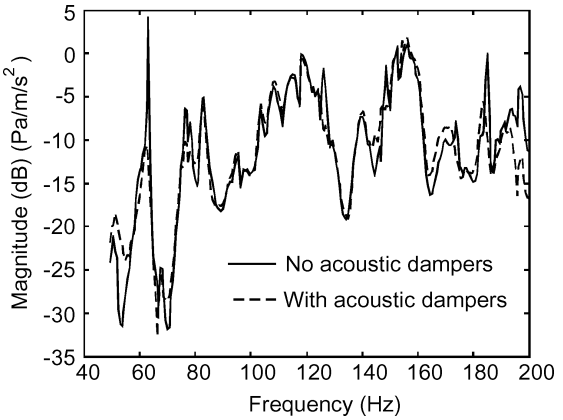

Fig. 19 Spatially averaged microphone measurement using acoustic dampers.

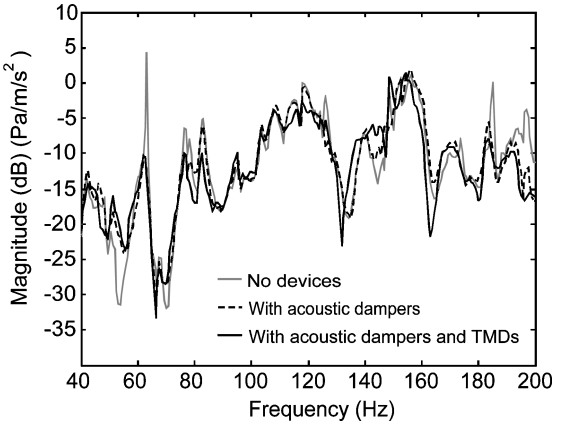

Fig. 20 Microphone measurements using all acoustic dampers compared to using all acoustic dampers with TMDs.

TVAs. For the case of the 196-Hz TMDs with all acoustic dampers, the reduction at the wall microphones was a comparable 1.56 dB, the reduction at the wall accelerometers was 0.87 dB (largest reduction achieved over the test cases), and the reduction at the tree microphones was 0.97 dB (also the largest reduction achieved over the test cases). Figure 20 shows the measured data for this test case. It appears that the TMD was able to produce damping at more than the target mode. From 180 to 200 Hz, there was less transmission with the TMDs than without. There was also less transmission near 84 Hz and 110–120 Hz, with little spillover elsewhere.

For comparison purposes, six solid aluminum blocks of equivalent mass and geometry were substituted for the 84 Hz TVAs using the same attachment locations and method. Measurements were taken using all acoustic dampers and showed 1.49 dB of reduction at the wall microphones, 0.72 dB of reduction at the tree microphones, and an increase of 0.63 dB at the wall accelerometers.

The data showed that significant attenuation of the low-frequency acoustic modes was accomplished using damped acoustic resonators. It was observed through additional testing that the influence of the acoustic dampers was somewhat robust to mistuning ($\pm 5\%$ of the resonance frequency). Including the TMD/TVAs increased the noise reduction provided by the resonators alone. The TMD/TVAs provided more reduction than did simple blocking masses. The TMDs provided the highest amount of reduction at the tree microphones and demonstrated a wider bandwidth of influence than their narrowband counterparts (TVAs). The TMDs were more robust to mistuning than the TVAs, which makes them more suitable for a system whose dynamics might vary.

The narrowband and wide-band performance observed in these tests met expectations. Both the acoustic and structural devices functioned as expected. However, after reflecting on the sensitivity of the structural resonance frequencies to boundary conditions and the

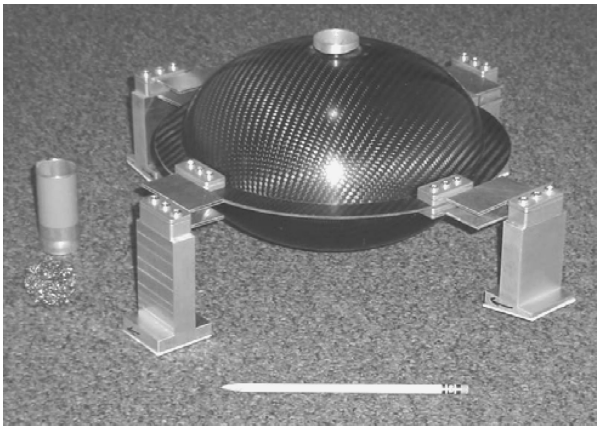

Fig. 21 PVAD used in integrated tests on the Boeing cylinder.

uncertainty in the transmission dynamics attributable to the disturbance coupling, it was decided that targeting specific structural modes with TVAs or TMDs was not reasonable because accurate knowledge of the cylinder's dynamic response was required, which might not be available for fairing applications. It was decided to instead use a relatively low frequency (50–80 Hz), damped suspension, with a damped acoustic resonator (as the TMD's moving mass) for the integrated PVAD. It was theorized that if the suspension were designed for low-frequency, structural damping could be imparted over a broad range of frequencies proximal to the design frequency. Knowledge of the structural dynamics can be less precise and good performance can still be achieved.

V. Integrated PVAD Development

The final PVAD design was constructed based on lessons learned from all of the previous numerical studies and experimental testing. The acoustic damper was designed to have a fundamental frequency of 63 Hz, which could be adjusted to 105 Hz by varying the neck length. Acoustic damping was designed to be 7%, which was achieved by installing approximately 5 g of copper mesh into the neck. The acoustic resonator volume was built from two carbon-fiber composite halves to form a 4500-cm^3 ellipsoid with a 2.5-cm-wide circumferential ring and an epoxied neck sleeve (shown in Fig. 21). The neck sleeve permitted the use of a neck tube that could be cut to the appropriate length and reinserted. This enabled easy tuning of the resonator frequency. The mass of the acoustic resonator was approximately 400 g.

The suspension system consisted of two rings of four S-shaped stainless-steel leaf springs separated by 2.4-cm spacers and mounted to four aluminum standoffs. The dual S-flexure ring approach was used to provide large frequency separation between the fundamental bounce mode of the PVAD and the other twisting and tilting modes (to prevent unexpected and/or undesired coupling). The design frequency for the suspension was 80 Hz. Finite element models were used to design the appropriate flexures, which turned out to be 0.8-mm stainless-steel flexures. By removing one ring of flexures, so that only four were used, the suspension frequency could be reduced to 50 Hz. Flexure damping of approximately 7% was achieved using constrained layer damping treatments. The standoffs to which the flexures were attached were constructed of aluminum. The bases of the standoffs were curved to match the curvature of the cylinder. Each integrated device weighed about 1.2 kg (largely because of the weight of the standoffs) and was attached to the cylinder by adhesive pads on the base of the standoffs. Thirty-five PVADs were constructed for testing on the composite cylinder.

VI. Integrated PVAD Testing

A. Foam Lining and Baseline Tests

In the previous acoustic resonator and TVA/TMD test results, it was observed that the interior acoustic response was much more lightly damped than occurred in actual payload fairings, which could give unrealistic expectations for performance in actual applications. Thus, for the integrated tests a representative acoustic blanket treatment was applied to the cylinder's interior so that the acoustic response more accurately represented actual fairing behavior. Melamine acoustic foam (5 cm thick) was incrementally added to the cylinder's interior until the measured acoustic damping ratios were similar to the damping response observed in a nominal Delta payload fairing. The foam had little mass loading effect on the structure, but did provide some structural damping. Figure 22 shows the sum squared of the measured transfer functions from an external disturbance source (subwoofer) to several internal microphones (an accelerometer on the subwoofer diaphragm was used as the reference). Approximately 16% of the surface area of the interior was covered with foam.

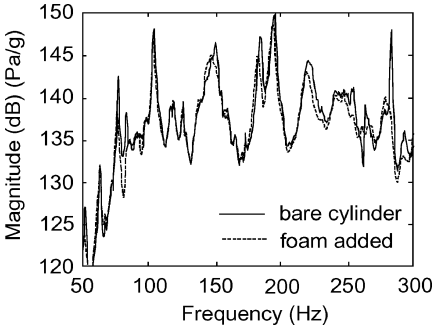

Fig. 22 Effect of added foam to the cylinder's interior for integrated testing.

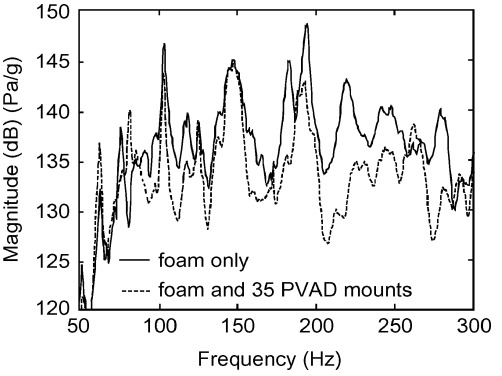

Fig. 23 Baseline acoustic response using foam and PVAD standoffs.

Another concern was the impact of the added mass of the PVAD standoffs on the cylinder's response. Thus, a "baseline" response was defined with the foam and with 35 sets of PVAD standoffs attached to the cylinder. Figure 23 shows the baseline noise transmission with foam and with the standoffs. The increased mass reduced the transmission at higher frequency as expected. At the fundamental acoustic mode 63 Hz, transmission increased, which was observed in simulations (see Fig. 6).

B. Test Setup: Equipment Description

Testing was performed in a larger test chamber than used for the previous studies. A sketch of the setup is presented in Fig. 24. The disturbance source was positioned approximately 2 m from the cylinder and generated a somewhat diffuse loading on the cylinder over the bandwidth of 40–300 Hz. (The loading was not truly diffuse; however, because the cylinder was in a reverberant lab, the impinging sound field consisted of reflected waves in addition to the direct wave field from the source. Also, the room was large and had scattering surfaces; thus, there were no dominant acoustic room modes that might bias the internal response. Measurements were made to measure the external acoustic levels around the circumference of the cylinder and indicated that the acoustic load was reasonably "even" around the cylinder, as opposed to being high on the side of the source, which would have indicated a primarily direct-field loading.) The disturbance level was approximately 103 dB for these tests. An accelerometer attached to the subwoofer

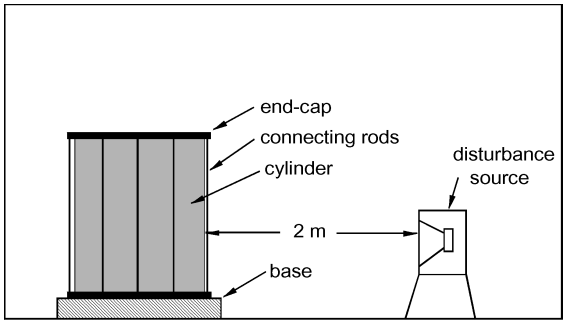

Fig. 24 Experimental setup for integrated device testing.

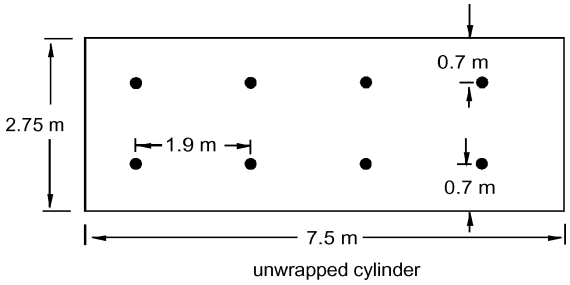

Fig. 25 Position of the external microphones around the "unwrapped" cylinder.

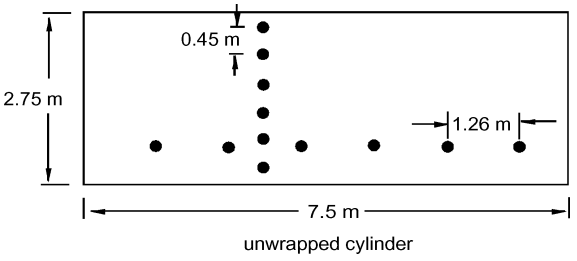

Fig. 26 Position of the accelerometers around the unwrapped cylinder.

diaphragm provided the reference measurement [PCB Piezotronics accelerometer model 352B10; sensitivity = 10 mV/g; frequency range = 2–10,000 Hz (±5%); mass = 0.5 g]. Bandlimited random noise was used as the disturbance input instead of burst chirps. These tests were conducted by graduate students and research associates of Virginia Tech (Vibration and Acoustics Laboratory, Department of Mechanical Engineering) using different acquisition and analyzer equipment than used in previous tests.

Eight external microphones [PCB Piezotronics ICP microphone model 130D20; sensitivity = 45 mV/Pa; frequency range = 20 Hz–7 kHz (±1 dB)] were placed around the cylinder exterior as shown in Fig. 25. These were used to monitor the external loading. Twelve accelerometers [PCB Piezotronics accelerometer model 320C03; sensitivity = 10 mV/g; frequency range = 1 Hz–6 kHz (±5%)] were attached to the cylinder exterior as shown in Fig. 26. Fourteen internal microphones [PCB Piezotronics ICP microphone model 130D20; sensitivity = 45 mV/Pa; frequency range = 20 Hz–7 kHz (±1 dB)] were mounted inside of the cylinder on wires. All measurements were high-pass filtered and antialias filtered. At least 20 averages of the transfer functions were taken for each test. Many different tests were completed over several weeks. In most cases, tests were repeated in order to better understand and quantify experimental uncertainty.

C. PVAD Layout

The layout of the PVADs is shown in Fig. 27 with the positions of the added acoustic foam indicated. The upper and lower rings were positioned near the end caps (locations of the acoustic pressure antinodes), which facilitated good coupling with the acoustic volume. The middle ring was positioned near the midspan of the cylinder, which was a location of relatively strong out-of-plane motion. The upper and lower rings each included 14 PVADs, and the middle ring included seven PVADs.

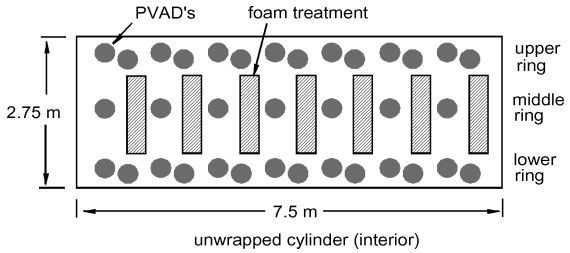

Fig. 27 PVADs and foam layout used in the integrated tests.

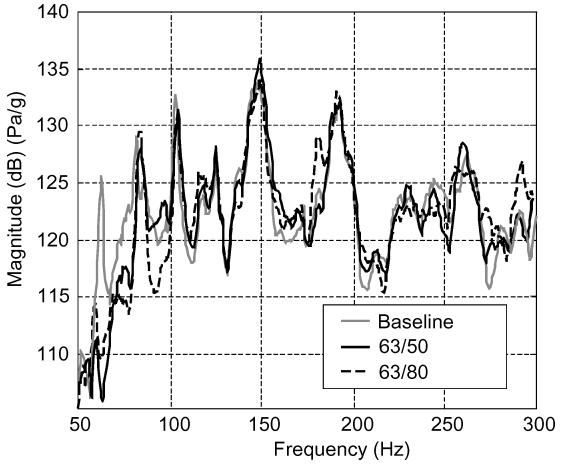

Fig. 28 Comparison of 35 PVADS tuned to 63/50 and 63/80 (Hz).

D. Results

1. Results: 35 PVADs with Varying Acoustic and Structural Resonance Frequency

The first set of tests compared the performance of 35 PVAD devices tuned to two different acoustic and two different structural resonance frequencies. Performance was measured over six narrow bandwidths around dominant transmission frequencies, and over the 50- to 300-Hz bandwidth. The noise reduction was computed as a function of the ratio of the spatially averaged response of the baseline case (with 35 sets of standoffs) to the response with the devices attached (dampers and flexures). Representative responses are presented, and the noise reduction values are tabulated for the averaged measurements and presented in Table 4.

First, the acoustic dampers were tuned to approximately 63 Hz (the fundamental acoustic mode of the cylinder), and the flexures were tuned to 50 Hz. This was compared to using the same acoustic resonance, but setting the flexures to 80 Hz. The spatially averaged transfer functions for a representative test run are given in Fig. 28. The results for the acoustic dampers with 50-Hz suspensions, denoted as 63/50, showed reduction below 80 Hz, but some spillover at 149 and 260 Hz. The 63/80 configuration yielded more reduction below 100 Hz, but no reduction at 84 Hz, and noticeable spillover at 180, 190, and 290 Hz. In both cases, the response at 63 Hz was reduced by more than 10 dB. Narrowband reductions are given in Table 4 and indicate that reduction typically occurred below 110 Hz. The computed reduction over the 50- to 300-Hz bandwidth for the 63/50 configuration was only about 0.27 dB, but the measurement uncertainty (based on standard deviation of the data) was 0.26 dB. For the 63/80 configuration, the reduction was slightly better at 0.37 dB (±0.11 dB).

Figure 29 compares the results using an acoustic damper tuned to 103 Hz, with the structural resonance tuned to 50 Hz (103/50) and 80 Hz (103/80). In this case, reduction was observed at resonances up to 145 Hz, with spillover occurring at 150, 180, 260, and 290 Hz. The 103/80 devices yielded more reduction than the 103/50 devices below 100 Hz. Reductions at 63 Hz were less than the previous case, but there were significant improvements at 84 and

Table 4 Narrowband and overall reduction (dB) measured using 35 PVADs with varying structural and acoustic frequencies

Bandwidth	f_c, Hz	$f_{\min} - f_{\max}$, Hz	63/50, dB	63/80, dB	103/50, dB	103/80, dB
1	62.5	57.5–67.5	11.30 ± 0.39	8.79 ± 0.30	5.89 ± 0.94	5.90 ± 0.81
2	80	75–90	2.05 ± 0.80	1.42 ± 0.84	4.21 ± 0.73	6.19 ± 0.62
3	105	100–110	1.65 ± 0.64	1.47 ± 0.23	5.79 ± 0.33	4.74 ± 2.39
4	125	120–130	0.75 ± 0.11	-0.17 ± 0.08	1.90 ± 0.13	1.30 ± 0.08
5	150	145–155	-0.97 ± 0.20	0.79 ± 0.09	-0.52 ± 0.53	1.49 ± 0.06
6	185	180–190	0.84 ± 0.37	-0.74 ± 0.37	0.83 ± 0.77	1.49 ± 0.42
Sum	——	——	15.62 ± 2.50	11.56 ± 1.91	18.08 ± 3.41	21.1 ± 4.37
Overall (50–300 Hz)	——	——	0.27 ± 0.26	0.37 ± 0.11	0.76 ± 0.39	1.55 ± 0.25

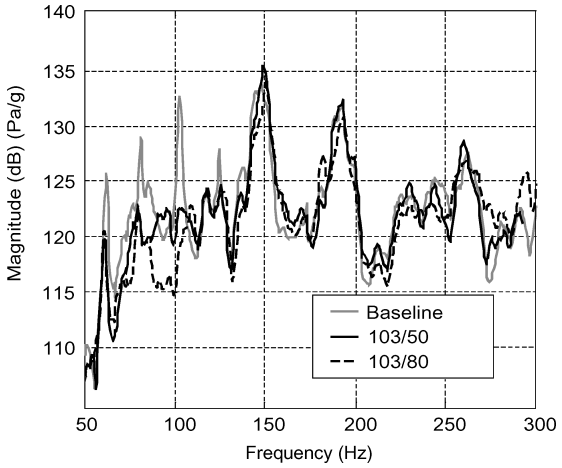

Fig. 29 Comparison of 35 PVADS tuned to 103/50 and 103/80 (Hz).

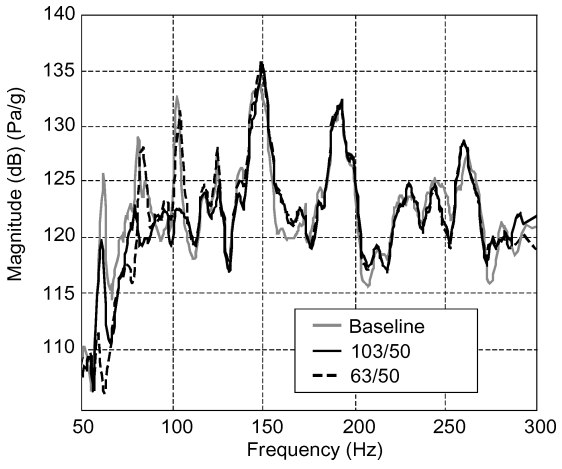

Fig. 30 Comparison of 35 PVADS tuned to 63/50 and 103/50 (Hz).

103 Hz. Table 4 shows that there were improved reductions over the six selected narrowbands and over the 50- to 300-Hz bandwidth. Clearly, the PVADs tuned to 103 Hz performed better than did the 63-Hz dampers, although less performance was realized at 63 Hz.

The next series of tests compared results obtained using a structural resonance frequency of 50 Hz, with the acoustic damper resonances set to either 63 or 103 Hz. The results are shown in Fig. 30. This reiterates that for a given suspension the 103-Hz dampers provided better attenuation over the bandwidth. Very little spillover was observed in this test. Figure 31 gives the results for the case of an 80-Hz structural resonance, with the acoustic damping switched between 63 and 103 Hz. Reduction below 100 Hz was greater than in the previous tests (Fig. 30), but more spillover at higher frequencies was observed.

The spatially averaged response measured at the accelerometers is presented in Fig. 32 for the 103/50 and 103/80 test cases. It shows that there were significant variations in the measured vibration levels between the two tests cases. Both configurations reduced vibration

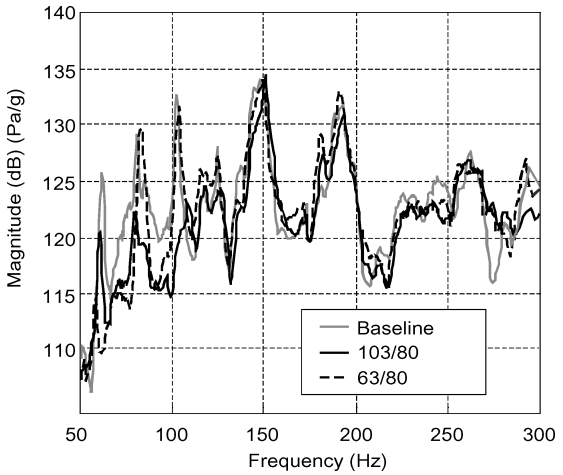

Fig. 31 Comparison of 35 PVADS tuned to 63/80 and 103/80 (Hz).

below 100 Hz, and the 80-Hz configuration reduced vibration up to 200 Hz (except from 150 to 160 Hz). The 50-Hz PVADs actually increased the vibration levels above 100 Hz. Both cases produced some spillover above 200 Hz. Mixed reduction and spillover was typical in all of the test cases. Note that at 103 Hz, the vibration level was increased by the 103/50 devices, but Fig. 29 shows that the acoustic response at 103 Hz was reduced by the 103/50 devices. Intuitively, one would expect increased acoustic response with increased vibration levels; however, here is a case of the opposite occurring. This shows that higher vibration levels do not necessarily imply higher acoustic levels, and likewise, lower vibration levels are not always indicative of lower acoustic response. It has been documented in the literature that vibration control does not necessarily translate into acoustic control. This is a realistic and expected consequence of the particular control mechanism utilized for reducing transmission. In some instances, one can reduce the overall vibration levels of the cylinder with little beneficial impact to the noise transmission. Conversely, by interrupting (or reconfiguring) the spatial vibration patterns of strong radiators (at a particular frequency), even without significant attenuation of the energy at that frequency, the radiation efficiency of a particular structural mode can be reduced, vibration of the cylinder can be decoupled from the acoustic volume, and transmission about that frequency can be significantly inhibited.

2. *Results: Varying Number of Devices*

In the final tests to be presented, the number of PVADs was varied, and the performance was measured as a function of the number of devices. Measurements were taken using 14 PVADs (the lower ring only), 21 PVADs (lower and middle rings), 28 PVADs (lower and upper rings), and compared to the full case of 35 PVADs (remeasured). The measured responses are presented in Figs. 33 and 34. The results given in Fig. 33 used acoustic dampers tuned to 63 Hz and flexures tuned to 80 Hz. For Fig. 34, the acoustic dampers were tuned to 103 Hz, and the flexures remained tuned to 80 Hz. These results were taken without a baseline reference, that is, no measurements were taken with only 14 sets of standoffs, 21 sets of standoffs, or 28

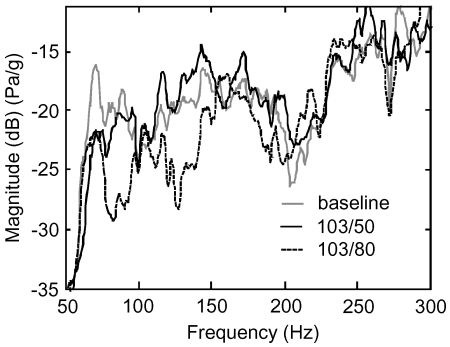

Fig. 32 Comparison of accelerometer measurements with 35 PVADS for two flexure resonances (acoustic resonance at 103 Hz).

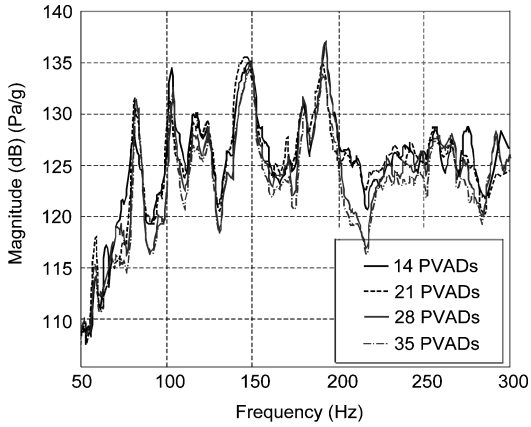

Fig. 33 Comparison of spatially averaged acoustic response as a function of the number of PVADs (63/80).

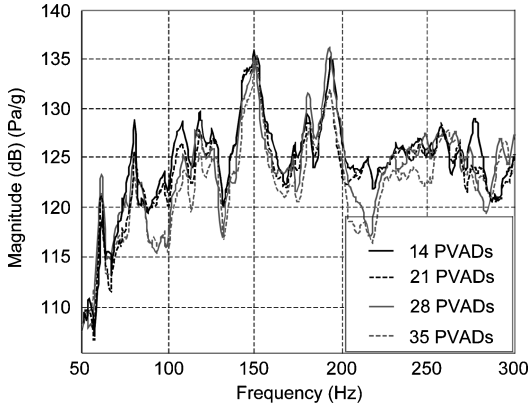

Fig. 34 Comparison of spatially averaged acoustic response as a function of the number of PVADs (103/80).

sets of standoffs. Figure 33 shows that 14 PVADs reduced the 63-Hz acoustic mode as effectively as 35 PVADs. There was no noticeable change observed at 84 Hz. At 103 Hz, 21 PVADs yielded more reduction than 14 PVADs, but no improvement was realized with 28 or 35 PVADs. There were no consistent trends above 150 Hz. In Fig. 34, 14 PVADs actually yielded more reduction than 28 PVADs. Above 63 Hz, the performance of 28 and 35 PVADs were reasonably similar, although 35 PVADs produce more reduction at 180, 190, and 250 Hz. The data do not indicate an optimal treatment. A considerable amount of the achievable reduction was achieved using 14 PVADs. Some gains were made using more devices, but that required a significant mass increase. The volume of 28 PVADs was equivalent to 1.0% of the total volume of the cylinder.

VII. Conclusions

The PVAD was developed to complement acoustic blankets to improve noise control at low frequencies and as a passive alternative to active noise control approaches for payload fairings. This work presented the development of the PVAD from prototype to an integrated device. Experimental results and analysis supported each stage of modeling and development. The final integrated device design was motivated in part by practical limitations and dynamic uncertainty in actual payload fairings. The result was a robust device to mitigate fairing noise using both structural and acoustic control.

Early work with prototype devices showed that although PVADs were designed with one acoustic and one structural resonance, they could be designed to couple with several proximal frequencies and provide wideband attenuation. Tests were conducted using both diaphragm-type and Helmholtz-resonator-type acoustic dampers. A PVAD weighing approximately 500 g was developed using a foam base and was successfully demonstrated in a one-dimensional aluminum cylinder test bed. It was estimated that the volume of the acoustic resonators needed to be approximately 1% of the total acoustic volume in order to provide significant levels of attenuation ("significant" meaning greater than 6 dB, i.e., a factor of 2, reduction in the amplitude of the response of the fundamental acoustic resonance).

Optimization studies that used fully coupled structural-acoustic finite element models of a 2.75-m graphite-epoxy, sandwich composite cylinder were presented. PVADs were coupled with the system model, and the simulations were used as tools to find optimal design parameters, locations, and predict the impact on noise transmission. Two optimization approaches were presented, one based on radiation-mode analysis and one that used genetic algorithms to seek optimal solutions. The simulations indicated that more devices would provide more attenuation, but as the number of devices increased, the rate of noise reduction decreased, that is, "diminishing returns." This was also observed in the integrated device tests, but to a lesser extent. Simulations indicated that using a flexible (dynamic) suspension yielded more reduction than simply attaching rigid (blocking) masses. The addition of acoustic dampers further reduced transmission. The optimal flexure and acoustic damping ratios of the PVADs were determined to be around 5 to 10% for the nominal system model. The optimal "moving mass" of the structural component tended toward the high end of the parameter space, and the optimal moving mass of the acoustic damper tended toward the low end of the parameter space. Simulations using damped Helmholtz resonators as acoustic dampers showed good performance. The locations of the PVADs on the cylinder wall did not seem to be as critical if many devices were used. However, if fewer devices were used then the PVADs tended toward locations that corresponded to high out-of-plane vibration and pressure antinodes.

Tests using separate components were conducted as a risk reduction step prior to the development and testing of integrated PVADs. Component tests demonstrated narrowband reductions of 10–12 dB at low-frequency acoustic resonances. Reactive structural devices provided narrowband attenuation, but resistive devices provided attenuation over a wider band with more robustness to mistuning. The measured results showed that the TVA/TMDs provided more reduction than did blocking masses. However, it was decided based on the uncertainty of a real fairing to not attempt to target specific structural resonances, but to design the flexure suspension near the low end of the target bandwidth, which resulted in attenuation over several resonance frequencies.

Integrated PVAD devices were constructed with adjustable flexures and acoustic dampers and then tested in the 2.75-m composite cylinder provided by Boeing. Acoustic foam was added to the cylinder's interior so that the acoustic damping was more representative of an actual payload fairing. Baseline frequency response functions were measured from a disturbance to several interior microphones and exterior accelerometers with the foam and PVAD legs attached. These frequency response functions were spatially averaged, and PVAD performance was computed relative to these baseline measurements.

Tests were conducted on the cylinder using 35 PVADs, all tuned to the same structural and acoustic frequencies. A variety of test cases were investigated and presented. The PVADs reduced "on-resonance" response, effectively coupled with several modes

over the low-frequency bandwidth, and produced little spillover. The performance of the PVADs correlated well with model predictions, with narrowband reductions of up to 11 dB measured at specific resonance frequencies. For the case of the 103/80 PVADs, there was significant (greater than 1 dB) reduction at all six bandwidths measured. The PVADs were particularly effective below 100 Hz, where acoustic blankets are least effective. Figure 29 showed performance through 130 Hz (more than two resonances). It is apparent that if some of the devices were changed from 103/80 to 150/80 and/or 190/80 significantly more reduction across the bandwidth might be realized. Furthermore, the added mass reduces transmission at higher frequency (>300 Hz). Additional testing should be done in which devices are implemented that cover a wider range of frequencies in order to assess potential effectiveness and limitations. Unfortunately for us, time and budget precluded this option.

In summary, the PVADs offer a viable passive solution for low-frequency noise control in flexible, structural-acoustic systems such as payload fairings. PVADs were reasonably robust to mistuning, placement, and damping values. PVADs can be constructed from lightweight composite materials (graphite-epoxy) with foam-based mounting/suspension systems that would weigh less than 500 g. Twenty such devices would add about 10 kg (22 lb) to a fairing. It is expected that improved wideband performance could be realized if the PVAD resonance frequencies were varied over the target bandwidth. Higher-frequency PVADs could be made smaller and lighter. Incorporating multiple PVADs with typical acoustic blankets would provide an effective broadband acoustic treatment for large payload fairings that exhibit large-amplitude, low-frequency resonant behavior. For smaller payload fairings, fewer PVADs (of smaller size) would be sufficient to provide significant noise reduction and reduce the payload vibroacoustic launch environment.

Acknowledgments

The authors acknowledge the support of the Air Force Office of Scientific Research for supporting this work. Also, we thank Haisam Osman of the Boeing Company for providing the composite cylinder used in these tests. We thank Colin Hansen, Ben Cazzolato, Anthony Zander, and Rick Morgans, all of the University of Adelaide, Adelaide, Australia, for their excellent work on genetic algorithms for passive vibroacoustic attenuation device (PVAD) optimization, which was also supported through the Air Force Office of Scientific Research/Asian Office of Aerospace Research and Development. We acknowledge the technical and laboratory support provided by Chris Fuller, Marty Johnson, James Carneal, and others at the Vibrations and Acoustics Laboratory at Virginia Polytechic Institute and State University (Virginia Tech). Finally, we thank Kyle Henderson of the U.S. Air Force Research Laboratory, Space Vehicles Directorate, for providing funding for the Virginia Tech effort and fabrication of the integrated PVADs.

References

[1]Doria, A., "Control of Acoustic Vibration of an Enclosure by Means of Multiple Resonators," *Journal of Sound and Vibration*, Vol. 181, No. 4, 1995, pp. 673–685.

[2]Yoda, K., and Konishi, S., "Tunable Acoustic Absorbing System for Semi-Active Noise Control," AIAA Paper 2000-2040, June 2000.

[3]Bies, D. A., and Hansen, C. H., *Engineering Noise Control: Theory and Practice*, 2nd ed., E & FN Spon, New York, 1996, Chap. 10, pp. 399–430.

[4]Inman, D. J., *Engineering Vibration*, 2nd ed., Prentice–Hall, 2001, Chap. 5, pp. 377–390.

[5]Marcotte, P., Fuller, C., and Johnson, M., "Numerical Modeling of Distributed Active Vibration Absorbers for Control of Noise Radiated by a Plate," *Proceedings of ACTIVE 2002, The 2002 International Symposium on Active Control of Sound and Vibration*, Univ. of Southampton, Southampton, England, U.K., 2002, pp. 535–546.

[6]Fuller, C. R., Maillard, J. P., Mercadal, M., and von Flotow, A. H., "Control of Aircraft Interior Noise Using Globally Detuned Vibration Absorbers," *Journal of Sound and Vibration*, Vol. 203, No. 5, 1997, pp. 745–761.

[7]O'Regan, S., Burkewitz, B., Fuller, C. R., Lane, S. A., and Johnson, M., "Payload Noise Suppression Using Distributed Active Vibration Absorbers," *Proceedings of SPIE*, Vol. 4698, edited by A. R. McGowan, Society of Photo-Optical Instrumentation Engineers (International Society for Optical Engineering), Bellingham, WA, 2002, pp. 150–159.

[8]Jolly, M. R., and Sun, J. Q., "Passive Tuned Vibration Absorbers for Sound Radiation Attenuation from Panels," *Proceedings of the SPIE*, Vol. 2193, edited by C. D. Johnson, Society of Photo-Optical Instrumentation Engineers (International Society for Optical Engineering), Bellingham, WA, 1994, pp. 194–201.

[9]Von Flotow, A. H., Beard, A., and Bailey, D., "Adaptive Tuned Vibration Absorbers: Tuning Laws, Tracking Agility, Sizing, and Physical Implementations," *Proceedings of the 1994 National Conference on Noise Control Engineering*, Vol. 1, edited by J. M. Cuschieri, Inst. of Noise Control Engineering, Poughkeepsie, NY, 1994, pp. 437–454.

[10]Carneal, J. P., Charette, F., and Fuller, C. R., "Minimization of Sound Radiation from Plates Using Adaptive Tuned Vibration Absorbers," *Journal of Sound and Vibration*, Vol. 270, No. 4–5, 2004, pp. 781–792.

[11]Esteve, S., and Johnson, M., "Reduction of Sound Transmission into a Circular Cylindrical Shell Using Distributed Vibration Absorbers and Helmholtz Resonators," *Journal of the Acoustical Society of America*, Vol. 112, No. 6, 2002, pp. 2840–2848.

[12]Osman, H., Johnson, M., Fuller, C., and Marcotte, P., "Interior Noise Reduction of Composite Cylinders Using Distributed Vibration Absorbers," AIAA Paper 2001-2230, 2001.

[13]Gardonio, P., Ferguson, N., and Fahy, F., "Modal Expansion Analysis of Noise Transmission Through Circular Cylindrical Shell Structure with Blocking Masses," *Journal of Sound and Vibration*, Vol. 244, No. 2, 2001, pp. 259–297.

[14]Pinder, J. N., and Fahy, F. J., "A Method for Assessing Noise Reduction Provided by Cylinders," *Proceedings of the Institute of Acoustics*, Vol. 15, 1993, pp. 195–205.

[15]Griffin, S., Lane, S. A., Hansen, C., and Cazzolato, B., "Active Structural Acoustic Control of a Rocket Fairing Using Proof-Mass Actuators," *Journal of Spacecraft and Rockets*, Vol. 38, No. 2, 2001, pp. 219–225.

[16]Griffin, S., and Lane, S. A., "Passive Vibroacoustic Attenuator for Structural Acoustic Control," U.S. Patent 6,195,442, filed 27 Aug. 1999; issued 27 Feb. 2001.

[17]Griffin, S. F., Gussy, J., Lane, S., Kemp, D., and Clark, L., "Innovative Passive Mechanisms for Control of Sound in a Launch Vehicle Fairing," *Collection of Technical Papers—AIAA/ASME/ASCE/AHS/ASC Structures, Structural Dynamics, and Materials Conference*, Vol. 1, No. 1, AIAA, Reston, VA, 2000, pp. 741–748.

[18]Cunnefare, K. A., and Currey, M. N., "On the Exterior Acoustic Radiation Modes of Structures," *Journal of the Acoustical Society of America*, Vol. 96, No. 4, 1994, pp. 2302–2312.

[19]Gibbs, G., Clark, R., Cox, D., and Vipperman, J., "Radiation Modal Expansion: Application to Active Structural Acoustic Control," *Journal of the Acoustical Society of America*, Vol. 107, No. 1, 2000, pp. 332–339.

[20]Clark, R., and Fuller, C., "Modal Sensing of Efficient Acoustic Radiators with Polyvinylidene Fluoride Distributed Sensors in Active Structural Acoustic Control Approaches," *Journal of the Acoustical Society of America*, Vol. 91, No. 6, 1992, pp. 3321–3329.

[21]*Matlab, The Language of Technical Computing*, ver. 6, Release 12, The Math Works, Inc., Natick, MA, 1984.

[22]Fahy, F. J., *Sound and Structural Vibration: Radiation, Transmission and Response*, Academic Press, New York, 1985, Chap. 6, pp. 241–267.

[23]*Genetic Algorithm and Direct Search Toolbox for Matlab*, ver. 1.0.1, The Math Works, Inc., Natick, MA, 2004.

[24]Lindner, D. K., Zvonar, G. A., Kirby, G. C., and Emery, G. M., "Genetic Algorithm Optimization of Feedback Control Systems," *Proceedings of the SPIE*, Vol. 2715, edited by V. V. Varadan and J. Chandra, Society of Photo-Optical Instrumentation Engineers (International Society for Optical Engineering), Bellingham, WA, 1996, pp. 543–554.

[25]Katsikas, S. K., Tsahalis, D., Manolas, D., and Xanthakis, S., "A Genetic Algorithm for Active Noise Control Actuator Positioning," *Mechanical Systems and Signal Processing*, Vol. 9, No. 6, 1995, pp. 697–705.

[26]Sadri, A. M., Wright, J. R., and Wynne, R. J., "Modeling and Optimal Placement of Piezoelectric Actuators in Isotropic Plates Using Genetic Algorithms," *Smart Materials and Structures*, Vol. 8, No. 4, 1999, pp. 490–498.

[27]Curtis, A. R. D., "An Application of Genetic Algorithms to Active Vibration Control," *Journal of Intelligent Material Systems and Structures*, Vol. 2, No. 4, 1991, pp. 472–481.

[28]Simpson, M. T., and Hansen, C. H., "Use of Genetic Algorithms for Optimizing Vibration Actuator Placement for Minimizing Sound Transmission into Enclosed Spaces," *Proceedings of SPIE, Smart Structures and Materials*, Vol. 2717, edited by I. Chopra, Society of Photo-Optical Instrumentation Engineers (International Society for Optical Engineering), Bellingham, WA, 1996, pp. 409–421.

[29]*ANSYS*, ver. 8.1, ANSYS, Inc., Canonsburg, PA, 2004.

L. Peterson
Associate Editor